Inorganic Chemistry

Article

pubs.acs.org/IC

$NaBa_2Cu_3S_5$: A Doped p-Type Degenerate Semiconductor

Mihai Sturza,[†] Fei Han,[†] Daniel P. Shoemaker,[†] Christos D. Malliakas,[†,‡] Duck Young Chung,[†] Hosub Jin,[§] Arthur J. Freeman,[§] and Mercouri G. Kanatzidis*[,†,‡]

[†]Materials Science Division, Argonne National Laboratory, Argonne, Illinois 60439, United States

[‡]Department of Chemistry and [§]Department of Physics and Astronomy, Northwestern University, Evanston, Illinois 60208, United States

Supporting Information

ABSTRACT: Mixed S^{2-}/S^{1-} oxidation states have been discovered in the new quaternary compound $NaBa_2Cu_3S_5$. Synthesized from the reaction of Cu in a molten alkali metal/polysulfide flux, the compound crystallizes in monoclinic space group $C2/m$ with a = 16.5363(7) Å, b = 5.5374(5) Å, c = 10.3717(10) Å, β = 98.535(8)°. The Na^+ Ba_2^{+2} $[Cu^+_3S_3]^{3-}S_2^{2-}$ crystal structure contains layers of edge sharing CuS_4 tetrahedra and sheets of S_2^{2-} dimers. These layers are separated by mixed Ba/Na cation layers. The conductivity of the single crystals of $NaBa_2Cu_3S_5$ is ~450 S cm^{-1} at room temperature, and increasing conductivity with decreasing temperature is observed, indicating metallic behavior despite the optical band gap of 0.45 eV. A small positive thermopower (45−55 μV K^{-1} from 300 K to 500 K) and Hall effect measurements also confirm p-type conductivity with carrier concentration at 200 K of ~1.6 × 10^{21} cm^{-3} and a hole mobility of ~2 cm^2 V^{-1} s^{-1}. $NaBa_2Cu_3S_5$ exhibits temperature-independent Pauli paramagnetism.

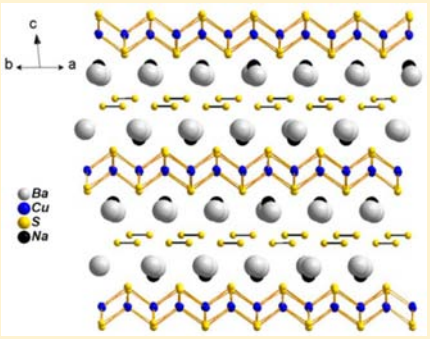

INTRODUCTION

The copper chalcogenide family consists of a relatively large number of binary and ternary members and has had a significant impact in energy applications as some of the leading photovoltaic materials.[1] Ternary copper chalcogenides can be divided into two groups: compounds with chain structures (i.e., α-$K[CuS_4]$,[2] β-$K[CuS_4]$,[2] $Cs[CuS_6]$,[3] $Na_3Cu_4S_4$[4,5]) and compounds with layered structures (i.e., ACu_4Q_3; A = K, Rb, Cs, Tl; Q = S, Se;[6] $NaCu_4S_4$[7]). These materials may also be classified according to valence: some are valence-precise while assuming Cu^+ and S^{2-}, while others are not. Determination of the charge state of copper in chalcogenides is a complex problem because of the highly covalent character of the Cu-Q bonds (Q = S, Se, Te) and the comparable energies of Cu d and Q p orbital states. There is general agreement that the mixed valence is generated mainly by oxidation of the chalcogen sublattice and not of copper(I), the maximal oxidation number per chalcogen atom varies from −2 (without chalcogen-chalcogen bonding) to ~−1.5.[8] Thus, virtually all valence-precise copper chalcogenides are semiconductors, whereas mixed-valent copper chalcogenides possess metallic conductivity.

In thiocuprates,[8] $[M_n]^{z+}[Cu_mS_n]^{z-}$, the anionic sublattice can be isolated anions or polymeric one-, two- or three-dimensional entities, often leading to anisotropy in the crystal structure and transport properties. The coordination geometry of copper can vary from linear (in $Na_4Cu_2S_3$,[9] KCuS,[10] $CsCu_3S_2$[11]), to trigonal planar or distorted flat trigonal pyramidal (in $Na_3Cu_4S_4$,[5] $Na_7Cu_{12}S_{10}$,[12] $Na_2Cu_4S_3$,[13] α-$BaCu_4S_3$,[14] MCu_3S_2 (M = K, Cs, Rb, Tl),[15−18] $M_3Cu_8S_6$ (M = K, Rb),[19] $MCu_{7-x}S_4$ (M = NH_4, K, Rb, Tl),[20−22] β-$CsCu_5S_3$[23]), distorted tetrahedral (in $TlCu_2S_2$,[24] β-$BaCu_2S_2$,[25] $MCu_{2n}S_{n+1}$,[26] $TlCu_6S_4$,[27] β-$BaCu_4S_3$[14]) or more complex framework structures (in $NaCu_5S_3$,[28] $BaCu_{5.65}S_{4.5}$,[29] $NaCu_4S_4$[7]). There is no clear-cut difference in the crystal structures of valence-precise and mixed-valence phases, and most thiocuprates are quite stable in air. The mixed-valence compounds have been of particular interest and subject to numerous synthetic, physical, and theoretical investigations because they exhibit interesting properties, such as metallic conductivity,[30,31] superconductivity,[32−34] and charge-density waves.[35]

The copper oxide family, such as YBCO ($YBa_2Cu_3O_{7-x}$) and LSCO ($La_{2-x}Sr_xCuO_4$), has had a huge impact on the development of the field of high-temperature superconductivity.[36−39] The list of unconventional superconductors has recently been expanded by the discovery of the ternary iron pnictides LnFeAs(O,F),[40] (Ln = rare earth elements), $Ba_{1-x}K_xFe_2As_2$[41−44] and chalcogenides $K_xFe_{2-y}Se_2$.[45−48] Interestingly, all these materials share two common features: (a) an infinitely extended square sublattice featuring anti-PbO type tetrahedral metal centers, for example, $[Fe_2As_2]$, $[Fe_2Se_2]$, and (b) mixed valency in the transition metal. Superconductivity in copper chalcogenides is rare with CuS,[49] CuS_2,[50] and $CuRh_2S_4$[51] being examples. A structurally analogous set of compounds to $Ba_{1-x}K_xFe_2As_2$ is $Ba_{1-x}K_xCu_2S_2$ which was described by Zhang, X. et al. and Mouallem-Bahout, M. et al.[52,53] The latter has the same anti-PbO-type sublattice in its $[Cu_2S_2]$ layer as the superconducting pnictides. While the doping substitution of K^+

Received: April 4, 2013
Published: June 3, 2013

   dx.doi.org/10.1021/ic4008284 | Inorg. Chem. 2013, 52, 7210−7217

ions for Ba^{2+} in the parent semiconducting compound $BaCu_2S_2$ creates mixed valency and metallic character, no superconductivity emerges. In an effort to investigate the electronic properties of the corresponding series $Ba_{1-x}Na_xCu_2S_2$ we discovered a new quaternary compound in the Ba−Na−Cu−S system with a novel structure and *p*-type metallic behavior. We report the synthesis, structure, and properties of a valence-precise but hole-doped phase, $NaBa_2Cu_3S_5$, which features anti-PbO-type $[Cu_2S_2]$ layers intercalated with Ba, Na cations and disulfide $[S_2^{2-}]$ anions.

EXPERIMENTAL SECTION

Reagents. The following reagents were used as received: (i) barium sulfide (99.9%, Sigma-Aldrich (ii) sodium sulfide (99.9%, Sigma-Aldrich), (iii) sulfur chunks, (99.999%, Spectrum Chemical Mfg. Corp.), (iv) Copper metal (99.9%, Sigma-Aldrich), (v) *N*,*N*′-dimethylformamide (DMF) and methanol analytical reagent.

Synthesis of $NaBa_2Cu_3S_5$. Synthetic preparations were carried out under a dry argon atmosphere in M-Braun glovebox. Initially, we had tried to prepare either $Ba_{1-x}Na_xCu_2S_2$ or $NaCu_4S_4$ by following the reported procedure:[7] a 9 mm diameter Pyrex tube containing Cu (0.032 g, 0.5 mmol), Na_2S (0.117 g, 1.5 mmol), BaS (0.042 g, 0.25 mmol), and S (0.096 g, 3 mmol) was evacuated and sealed under vacuum. The tube was heated at 500 °C for 4 days and then slowly cooled to 140 °C at 4 °C/h. Excess polysulfide flux was removed from the product with *N*,*N*′-dimethylformamide and methanol. Two kinds of crystals were found: black thin plate crystals of $NaBa_2Cu_3S_5$ (∼75% yield) and black thin needle crystals of $Na_3Cu_4S_4$ (∼25% yield) which was the major phase in literature.[4,5]

After the stoichiometry of the new quaternary compound was elucidated from the crystal structure determination (described subsequently), we directly synthesized $NaBa_2Cu_3S_5$ as a single phase using a stoichiometric mixture of Na_2S (0.039 g, 0.5 mmol), BaS (0.3387 g, 2 mmol), Cu (0.190 g, 3 mmol), and S (0.080 g, 2.5 mmol). The ground powders of these starting materials were loaded into a graphite crucible to avoid the reaction of sulfide with the glass. The graphite crucible was then placed inside a fused silica tube and flame-sealed under a pressure of $<10^{-4}$ mbar. The tube was then heated to 700 °C over 12 h and kept there for 24 h, and subsequently cooled slowly to room temperature at a rate of 10 °C/h.

Single Crystal X-ray Diffraction. Single crystals were selected and mounted on tips of glass fibers for X-ray diffraction. The data collection for a thin plate single crystal of $NaBa_2Cu_3S_5$ was performed at 150 K and room temperature. Intensity data were collected using ω scans on a STOE imaging plate diffraction system (IPDS-II) using graphite-monochromatized Mo−Kα radiation (λ = 0.71073 Å) operating at 50 kV and 40 mA with a 34 cm diameter imaging plate. Individual frames were collected with a 3 min exposure time and a 1° ω rotation. X-AREA, X-RED, and X-SHAPE[54] software packages were used for data collection, integration, and analytical absorption corrections, respectively, and SHELXL[55] and JANA2006[56] software packages were used to solve and refine the structure. The parameters for data collection and the details of the structure refinement are given in Table 1. Atomic coordinates, thermal displacement parameters (U_{eq}) and occupancies of all atoms are given in Table 2. Anisotropic displacement parameters and selected bond lengths and angles are given in Tables 3 and 4 for both compounds.

Powder X-ray Diffraction and Scanning Electron Microscopy. Phase purity of the products was confirmed by powder X-ray diffraction (XRD). The samples were finely ground and mounted on a flat plate sample holder to be analyzed with a Panalytical X'pert Pro diffractometer with an iron filtered Cu-Kα source, operating at 45 kV and 40 mA under a continuous scanning method in 2θ range of 5−120° and step size of 0.0167°. Powder XRD data were analyzed with the Rietveld method using the FULLPROF 2000 program.[57]

The semiquantitative microprobe analyses of several crystals were performed with a Hitachi S-2700 Scanning Electron Microscope using a Noran System Six Energy Dispersive Spectroscope (EDS) equipped with a thin window detector. Data were acquired by applying 20 kV of accelerating voltage. Semiquantitative analysis by EDS on several crystals indicated an average composition of $Na_{1.024(7)}Ba_{1.984(8)}Cu_{2.954(9)}S_{5.066(7)}$.

Table 1. Summary of Crystallographic Data and Structure Refinement for $NaBa_2Cu_3S_5$ at 293 K and 150 K

	$NaBa_2Cu_3S_5$	
formula weight	648.59	648.59
temperature	293(2) K	150(2) K
wavelength	0.71073 Å	0.71069 Å
crystal system	monoclinic	monoclinic
space group	*C*2/*m*	*C*2/*m*
unit cell dimensions	a = 16.5363(7) Å	a = 16.4865(1) Å
	α = 90.00°	α = 90.00°
	b = 5.5374(5) Å	b = 5.5188(3) Å
	β = 98.535(8)°	β = 98.534(5)°
	c = 10.3717(10) Å	c = 10.3300(7) Å
	γ = 90.00°	γ = 90.00°
volume	939.20(16) Å^3	929.48(10) Å^3
Z	4	4
density(calculated)	4.587 g/cm^3	4.635 g/cm^3
absorption coefficient	16.020 mm^{-1}	16.188 mm^{-1}
F(000)	1160	1160
crystal size (mm^3)	0.1551 × 0.1386 × 0.0626	0.1875 × 0.1606 × 0.0737
θ range for data collection	1.99 to 29.15°	1.99 to 29.15°
index ranges	$-22 \le h \le 22$,	$-22 \le h \le 22$,
	$-7 \le k \le 7$,	$-7 \le k \le 7$,
	$-14 \le l \le 13$	$-13 \le l \le 14$
reflections collected	4507	4464
independent reflections	1381 [R_{int} = 0.0532]	1369 [R_{int} = 0.0531]
completeness to θ = 29.15°	99.4%	99.6%
refinement method	full-matrix least-squares on F^2	
data/restraints/parameters	1381/0/61	1369/0/60
goodness-of-fit	1.100	1.077
final R indices [>2σ(I)]	R_{obs} = 0.0336, wR_{obs} = 0.0837	R_{obs} = 0.0305, wR_{obs} = 0.0768
R indices [all data]	R_{all} = 0.0377, wR_{all} = 0.0859	R_{all} = 0.0343, wR_{all} = 0.0786
largest diff. peak and hole	2.209 and −1.445 e·Å^{-3}	1.986 and −2.775 e·Å^{-3}

Differential Thermal Analysis (DTA). DTA measurements were carried out with a Shimadzu DTA-50 thermal analyzer. The ground sample (∼40 mg total mass) was sealed in a carbon coated fused silica ampule under vacuum. A silica ampule containing alumina of equal mass was sealed and placed as a reference. The sample was heated to 850 °C at 5 °C/min, followed by cooling at the same rate to 50 °C. The stability and reproducibility of the sample was monitored by running multiple heating and cooling cycles. Residues of the DTA experiments were examined with X-ray powder diffraction.

Raman Spectroscopy. A ground crystalline sample was loaded in a 0.5 mm diameter glass capillary for Raman spectroscopy analysis. A Renishaw inVia Raman microscope with a CCD detector was used to perform the measurement. The sample was irradiated by a 532 nm laser with data collected by 5 scans were averaged.

Infrared Spectroscopy and Band Gap Determination. The optical band gap of $NaBa_2Cu_3S_5$ was determined using optical diffuse-reflectance FT-IR spectroscopy. FT-IR spectra of the samples were recorded as a solid in KBr matrix. The spectra were recorded in the mid-IR (500−4000 cm^{-1}) regions with 4 cm^{-1} resolution by using a Nicolet 740 FT-IR spectrometer equipped with a TGS/PE detector and silicon beam splitter. Reflectance versus wavelength data were

dx.doi.org/10.1021/ic4008284 | Inorg. Chem. 2013, 52, 7210−7217

Table 2. Atomic Coordinates (×10^4) and Equivalent Isotropic Displacement Parameters (Å^2 × 10^3) of $NaBa_2Cu_3S_5$ at (a) 293(2) K and (b) 150(2) K with Estimated Standard Deviations in Parentheses

	Wyck	x	y	z	occupancy	U_{eq}[a]
			(a) $NaBa_2Cu_3S_5$ 293(2) K			
Ba(1)	4i	2637(1)	0	3024(1)	1	14(1)
Ba(2)	4i	4580(1)	−5000	2906(1)	1	14(1)
Cu(1)	4g	5000	−2388(2)	0	1	20(1)
Cu(2)	8g	1688(1)	2555(2)	−96(1)	1	21(1)
S(1)	4i	976(1)	0	1214(2)	1	12(1)
S(2)	4i	2613(1)	−5000	1475(2)	1	12(1)
S(3)	4i	4300(1)	0	1489(2)	1	12(1)
S(4)	8j	1241(1)	1906(2)	4708(2)	1	17(1)
Na	4i	3939(2)	0	7630(3)	1	21(1)
			(b) $NaBa_2Cu_3S_5$ 150(2) K			
Ba(1)	4i	7636(1)	0	3023(1)	1	7(1)
Ba(2)	4i	9578(1)	−5000	2906(1)	1	8(1)
Cu(1)	4g	5000	−2617(2)	0	1	10(1)
Cu(2)	8j	6688(1)	−2559(2)	−96(1)	1	10(1)
S(1)	8j	6241(1)	1914(2)	4701(1)	1	10(1)
S(2)	4i	5976(1)	0	1216(2)	1	6(1)
S(3)	4i	5701(1)	−5000	−1486(2)	1	7(1)
S(4)	4i	7612(1)	−5000	1471(2)	1	7(1)
Na	4i	6058(2)	−5000	2363(3)	1	11(1)

[a] U_{eq} is defined as one-third of the trace of the orthogonalized U_{ij} tensor.

Table 3. Anisotropic Displacement Parameters (Å^2 × 10^3) for $NaBa_2Cu_3S_5$ at (a) 293(2) K and (b) 150(2) K with Estimated Standard Deviations in Parentheses[a]

	U_{11}	U_{22}	U_{33}	U_{12}	U_{13}	U_{23}
			(a) $NaBa_2Cu_3S_5$ 293(2) K			
Ba(1)	11(1)	13(1)	17(1)	0	1(1)	0
Ba(2)	12(1)	13(1)	17(1)	0	4(1)	0
Cu(1)	18(1)	18(1)	22(1)	0	1(1)	0
Cu(2)	18(1)	20(1)	24(1)	0(1)	5(1)	2(1)
S(1)	8(1)	12(1)	15(1)	0	2(1)	0
S(2)	10(1)	10(1)	16(1)	0	2(1)	0
S(3)	10(1)	11(1)	16(1)	0	2(1)	0
S(4)	18(1)	17(1)	17(1)	−4(1)	2(1)	−2(1)
Na	15(2)	22(2)	27(2)	0	6(1)	0
			(b) $NaBa_2Cu_3S_5$ 150(2) K			
Ba(1)	4(1)	6(1)	11(1)	0	1(1)	0
Ba(2)	5(1)	7(1)	11(1)	0	2(1)	0
Cu(1)	7(1)	8(1)	13(1)	0	1(1)	0
Cu(2)	7(1)	9(1)	14(1)	0(1)	3(1)	−1(1)
S(1)	8(1)	9(1)	11(1)	−2(1)	2(1)	−1(1)
S(2)	2(1)	6(1)	9(1)	0	2(1)	0
S(3)	4(1)	5(1)	11(1)	0	2(1)	0
S(4)	4(1)	5(1)	12(1)	0	2(1)	0
Na	6(1)	13(2)	16(2)	0	4(1)	0

[a] The anisotropic displacement factor exponent takes the form: $-2\pi^2[h^2a^{*2}U_{11} + ... + 2hka^*b^*U_{12}]$.

used to estimate the band gap of the material by converting reflectance to absorption data according to the Kubelka–Munk equation, $\alpha/S = (1 - R)^2/(2R)$ where R is the reflectance and α and S are the absorption and scattering coefficients, respectively[58−61]

Electrical and Magnetic Properties. Variable temperature four probe resistivity and Hall effect measurements on single crystal samples of $NaBa_2Cu_3S_5$ were carried out by a Quantum Design PPMS. The temperature range was 5−300 K for resistivity and 2−200 K for Hall effect measurement. The Hall effect was measured by reversing the magnetic field $H = \pm 9$ T. Measurements were performed in four-probe geometry with 50 μm gold wires and silver paste used for the current and voltage electrodes, respectively. Above room temperature electrical resistivity and thermoelectric power measurements as a function of temperature were performed under vacuum using a custom setup including a Keithley Model 2182A nanovoltmeter and 6514 electrometer and MMR Technologies K-20 temperature controller. We used the integral method of measuring the Seebeck voltage $V(T)$, in which one end of the sample is held at a fixed temperature T_o, and the other end is varied through the temperature T range of interest. The Seebeck coefficient S is obtained from the slope of the $V(T)$ vs T curve, that is, $S = dV(T)/dT$.[62]

Magnetic susceptibility measurements were carried out with a Quantum Design MPMS SQUID magnetometer. Pieces of ground single crystals of $NaBa_2Cu_3S_5$ were loaded in a gelatin capsule. Temperature-dependent data were collected after zero field cooling (ZFC) and field cooling (FC) between 2 and 300 K, with applied field $H = 0.1$ T.

Band Structure Calculations. The band structure of $NaBa_2Cu_3S_5$ was studied by performing first-principles electronic structure calculations within the density functional theory framework. The plane-wave basis set was employed and a pseudopotential was generated using the projector augmented wave method[58] which is implemented in the Vienna Ab initio Simulation Package (VASP) code.[63−65] The cutoff energy for the plane-wave basis was set to 400 eV and regular k-point grids with density of 50 Å^{-1} was used for Brillouin zone sampling. For exchange-correlation functional, we employed the local density approximation (LDA) scheme.

RESULTS AND DISCUSSION

Synthesis. The single crystals of $NaBa_2Cu_3S_5$ were synthesized from a mixed Na/Ba/S flux which was initially intended to stabilize ternary $Na_3Cu_4S_4$[7] or create members of the series $Ba_{1-x}Na_xCu_2S_2$. After removal of the excess polysulfide flux with *N*,*N*′-dimethylformamide and methanol, thin plate-like black crystals of $NaBa_2Cu_3S_5$ (∼75% yield) and black thin needle crystals of $Na_3Cu_4S_4$ (∼25% yield) were observed. Once the phase $NaBa_2Cu_3S_5$ was identified by the single crystal structure and EDS analysis, a reaction of the stoichiometric mixture of Na_2S, BaS, Cu, and S was performed at 700 °C where the phase forms as a pure ingot of

dx.doi.org/10.1021/ic4008284 | Inorg. Chem. 2013, 52, 7210−7217

Table 4. Representative Bond Lengths (Å) and Bond Angles (deg) of $NaBa_2Cu_3S_5$ at (a) 293(2) K and (b) 150(2) K[a]

(a) $NaBa_2Cu_3S_5$ 293(2) K		(b) $NaBa_2Cu_3S_5$ 150(2) K	
Atom−Atom Bond Length			
Cu(1)−S(1)(×2)	2.3836(3)	Cu(1)−S(2)(×2)	2.3776(2)
Cu(1)−S(3)(×2)	2.4508(4)	Cu(1)−S(3)(×2)	2.4383(3)
Cu(2)−S(1)(×1)	2.3896(4)	Cu(2)−S(2)(×1)	2.3837(2)
Cu(2)−S(2)(×1)	2.4229(4)	Cu(2)−S(3)(×1)	2.4149(3)
Cu(2)−S(2)(×1)	2.4672(4)	Cu(2)−S(4)(×1)	2.4140(3)
Cu(2)−S(3)(×1)	2.4264(3)	Cu(2)−S(4)(×1)	2.4544(3)
Ba(1)−S(1)(×1)	3.0871(5)	Ba(1)−S(2)(×1)	3.0757(4)
Ba(1)−S(2)(×2)	3.1984(8)	Ba(1)−S(4)(×2)	3.1889(8)
Ba(1)−S(3)(×1)	3.3755(5)	Ba(1)−S(1)(×2)	3.2501(1)
Ba(1)−S(4)(×2)	3.2588(2)	Ba(1)−S(1)(×2)	3.2547(1)
Ba(1)−S(4)(×2)	3.2693(3)	Ba(1)−S(3)(×1)	3.3669(4)
Ba(2)−S(1)(×1)	3.1007(5)	Ba(2)−S(2)(×1)	3.0907(1)
Ba(2)−S(2)(×1)	3.3693(5)	Ba(2)−S(3)(×2)	3.1269(7)
Ba(2)−S(3)(×2)	3.1365(8)	Ba(2)−S(1)(×2)	3.1690(1)
Ba(2)−S(4)(×2)	3.1745(2)	Ba(2)−S(1)(×2)	3.2493(1)
Ba(2)−S(4)(×2)	3.2597(2)	Ba(2)−S(4)(×1)	3.3587(4)
Na−S(2)(×1)	2.855(3)	Na−S(1)(×2)	2.934(3)
Na−S(3)(×1)	2.920(3)	Na−S(2)(×2)	2.9982(2)
Na−S(4)(×2)	2.948(3)	Na−S(3)(×1)	2.906(3)
Na−S(1)(×2)	3.0119(4)	Na−S(4)(×1)	2.849(3)
S(4)−S(4)	2.110(3)	S(1)−S(1)	2.112(2)
Atom−Atom−Atom Bond Angle			
S(1)−Cu(1)−S(1)	105.28(6)	S(2)−Cu(1)−S(2)	105.19(5)
S(1)−Cu(1)−S(3)	108.30(4)	S(2)−Cu(1)−S(3)	109.99(5)
S(1)−Cu(1)−S(3)	109.93(5)	S(2)−Cu(1)−S(3)	108.26(4)
S(3)−Cu(1)−S(3)	114.70(5)	S(3)−Cu(1)−S(3)	114.72(5)
S(1)−Cu(2)−S(2)	107.95(4)	S(2)−Cu(2)−S(3)	108.84(5)
S(1)−Cu(2)−S(3)	108.92(5)	S(2)−Cu(2)−S(4)	107.85(4)
S(2)−Cu(2)−S(3)	108.21(5)	S(3)−Cu(2)−S(4)	108.41(5)
S(1)−Cu(2)−S(2)	104.98(5)	S(2)−Cu(2)−S(4)	105.06(5)
S(2)−Cu(2)−S(2)	114.01(4)	S(3)−Cu(2)−S(4)	112.55(4)
S(3)−Cu(2)−S(2)	112.55(4)	S(4)−Cu(2)−S(4)	113.90(3)

[a]Symmetry transformations used to generate equivalent atoms for (a) and (b): (1) *x*,*y*+1,*z* (2) −*x*+3/2,−*y*+1/2,−*z*+1 (3) −*x*+3/2,*y*−1/2,−*z*+1 (4) *x*,−*y*,*z* (5) −*x*+3/2,−*y*−1/2,−*z* (6) −*x*+3/2,*y*+1/2,−*z* (7) *x*+1/2,*y*−1/2,*z* (8) −*x*+3/2,−*y*−3/2,−*z* (9) −*x*+3/2,−*y*−1/2,−*z*+1 (10) *x*+1/2,−*y*−1/2,*z* (11) −*x*+3/2,*y*−1/2,−*z* (12) −*x*+1,−*y*,−*z* (13) −*x*+1,−*y*−1,−*z* (14) −*x*+1,*y*,−*z* (15) *x*−1/2,*y*+1/2,*z* (16) *x*,−*y*−1,*z* (17) *x*,*y*−1,*z* (18) *x*−1/2,*y*−1/2,*z*.

$NaBa_2Cu_3S_5$. The single-phase material was confirmed by the excellent match between the calculated and the experimental powder X-ray diffraction (XRD) patterns using Rietveld refinements. Results of Rietveld refinement, agreement factors, and refined lattice constants of powder X-ray diffraction patterns (Cu-Kα1 radiation) of the sample studied in this work are shown in Figure 1. The results are in good agreement (Bragg R-factor = 6.23, Rf-factor = 4.59) with the structure refined by single crystal X-ray diffraction. Despite its incongruent melting behavior (described below) we succeeded in growing millimeter size single crystals by slow cooling from the melt.

DTA experiments up to 850 °C at a rate of 5 °C/min on polycrystalline $NaBa_2Cu_3S_5$ show a single endothermic melting point around 630 °C and exothermic crystallization point around 580 °C in the heating−cooling cycle (Figure 2a). The sample after DTA was examined by XRD and showed the presence of $BaCu_2S_2$ and BaS, suggesting $NaBa_2Cu_3S_5$ melts incongruently (Supporting Information, Figure S1).

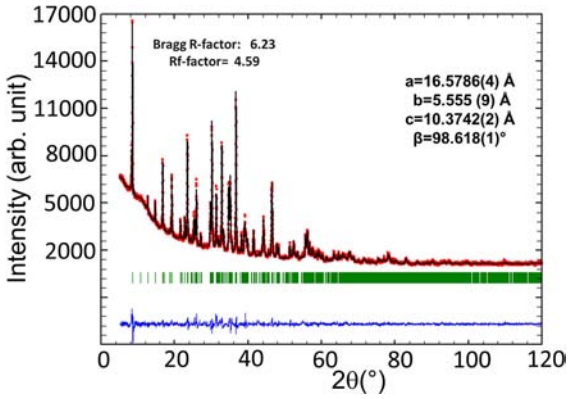

Figure 1. Calculated and observed XRD patterns of the Rietveld refinement for $NaBa_2Cu_3S_5$ (λ = 1.5406 Å, Bragg R-factor: 6.23%; Rf-factor = 4.59%).

Crystal Structure. The single-crystal structures of the new compound were determined at room temperature (293 K) and at 150 K. No structural transition between these two temperatures was found. The crystallographic data, selected bond distances, and bond angles for $NaBa_2Cu_3S_5$ at both temperatures are listed in Tables 1−4.

The black plate crystal of $NaBa_2Cu_3S_5$ crystallizes in the monoclinic space group *C*2/*m*, with cell parameters of *a* = 16.5363(7) Å, *b* = 5.5374(5)Å, *c* = 10.3717(10) Å, β = 98.535(8)°, and *Z* = 4. The layered structure of $NaBa_2Cu_3S_5$ projected onto the *ab*-plane is depicted in Figure 3a. The structure is built up of a two-dimensional network of anti-PbO type $[Cu_2S_2]$ layers, which are separated by the Ba and Na cations as well as disulfide $[S_2^{2-}]$ dimers. These disulfide groups are bonded only to the Ba and Na cations. The structure of the $[Cu_2S_2]^{2-}$ slabs is composed of tetrahedral Cu centers that share the edges to form the $[Cu_2S_2]^{2-}$ layer along the *ab* plane (Supporting Information, Figure S2). Since the disulfide units in the structure are not part of the Cu/S network (Figure 3c), the chemical formula can also be represented as a double salt $(NaBaCu_3S_3)\cdot BaS_2$.

There are two crystallographically independent Cu atoms in the structure, both tetrahedrally coordinated by S^{2-} atoms: Cu(1) by two S(1) and two S(3) and Cu(2) by two S(2), one S(1) and one S(3) atoms. All Cu−S bonds are normal and fall in the narrow range between 2.3836(3) and 2.4672(4) Å. The angles around Cu and S are close to those expected for distorted tetrahedral coordination in the ranges of 105.28(6)−114.70(5)° for S(1)−Cu(1)−S(1) and S(3)−Cu(1)−S(3) and 104.98(5)−112.55(4)° for S(1)−Cu(2)−S(2) and S(3)−Cu(2)−S(2) atoms, respectively.

The coordination environments of Na, Ba(1), and Ba(2) are shown in Figure 4a,b. Na^+ ions are situated within the atomic layers and surrounded by 6 S atoms with an average Na···S distance in the narrow range between 2.855(3) and 3.0119(4) Å. Two crystallographically distinct Ba^{2+} ions are located between the anionic layers. Both are octahedrally coordinated by 8 S atoms with an average Ba···S distance of 3.21(5) Å. The S(4)−S(4) distance of the disulfide unit 2.110(3) Å close to a S−S single bond at 2.09(1) Å found in $NaCu_4S_4$,[7] but shorter than the 2.15 Å found in CuS.[66,67] The Raman spectrum obtained from a powder of $NaBa_2Cu_3S_5$ (inset Figure 2b) shows a sharp peak at 470 cm^{-1} which corresponds to the S−S stretching modes of S_2^{2-} chains.[68−71] This measurement confirms the presence of S−S bonds that are implied by 2.15

dx.doi.org/10.1021/ic4008284 | *Inorg. Chem.* 2013, 52, 7210−7217

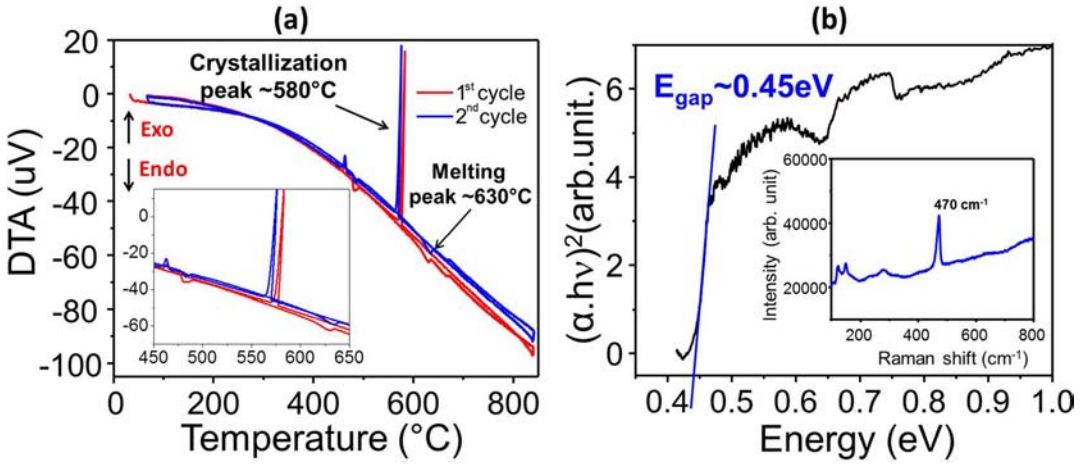

Figure 2. (a) DTA of $NaBa_2Cu_3S_5$ showing a single melting and crystallization behavior. (b) Diffuse reflectance FT-IR spectrum of $NaBa_2Cu_3S_5$ measured at room temperature, showing a band gap of 0.45 eV. The inset in (b) shows the room-temperature Raman spectrum of $NaBa_2Cu_3S_5$ with a peak around 470 cm^{-1} corresponding to the S–S stretching mode of S_2^{2-} units.

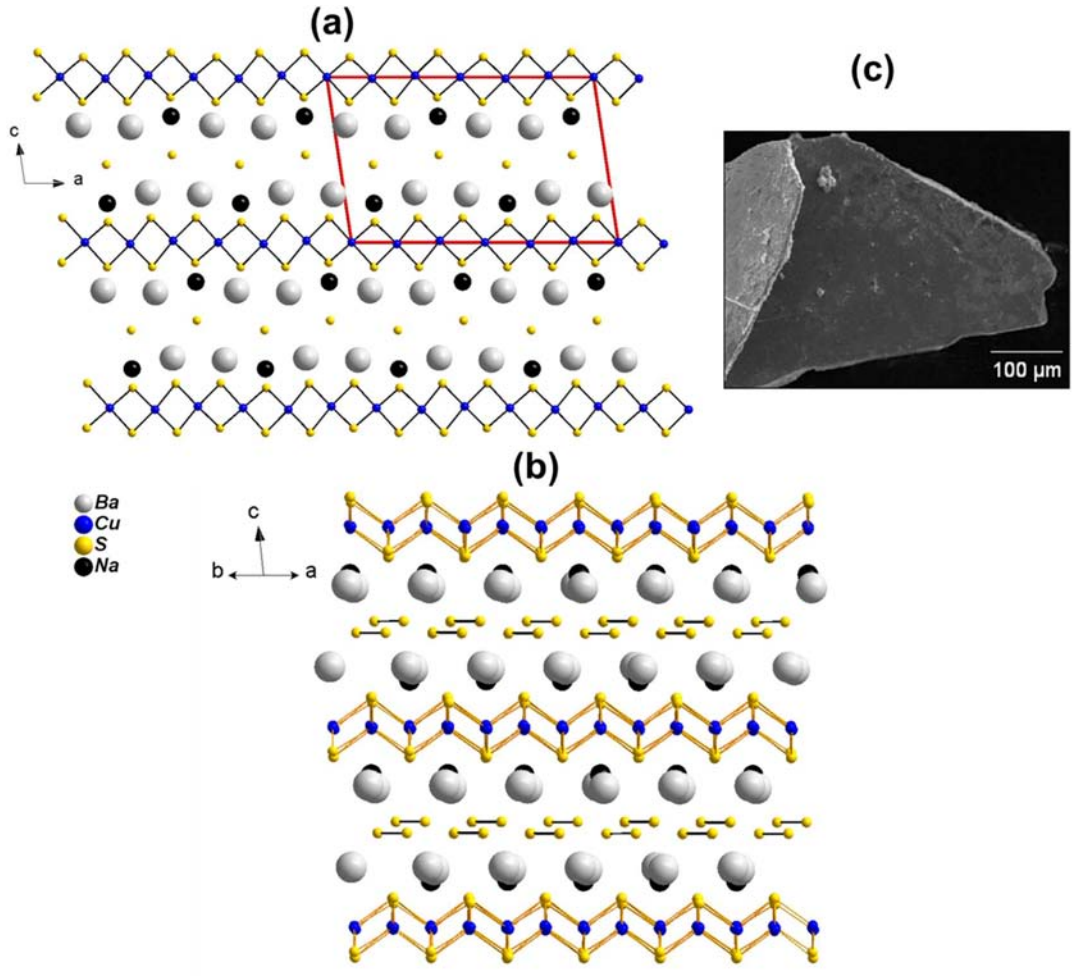

Figure 3. Perspective view of the layered structure of $NaBa_2Cu_3S_5$ (a) along and (b) perpendicular to crystallographic *b*-axis. Ba atoms are gray; Cu atoms blue, Na atoms black, and S atoms yellow. (c) SEM micrograph of a typical $NaBa_2Cu_3S_5$ crystal.

Å S–S distances in single crystal refinement. Assuming oxidation states of Cu atoms are 1+, the charge balances by $Na^+Ba^{2+}{}_2[Cu^+{}_3S_3]^{3-}S_2^{2-}$.

Physical Properties. *Optical Absorption Properties.* Based on the charge balanced formula of $Na^+Ba^{2+}{}_2[Cu^+{}_3S_3]^{3-}S_2^{2-}$ the compound is valence precise and is expected to be a semiconductor. FT-IR diffuse reflectance spectra collected for $NaBa_2Cu_3S_5$ at room temperature indeed reveal a band gap observed at ~0.45 eV, Figure 2b. This narrow energy gap is consistent with the black color of the crystals. The presence of a band gap in $NaBa_2Cu_3S_5$ is also predicted by ab initio theoretical calculations to be presented below.

dx.doi.org/10.1021/ic4008284 | *Inorg. Chem.* 2013, 52, 7210–7217

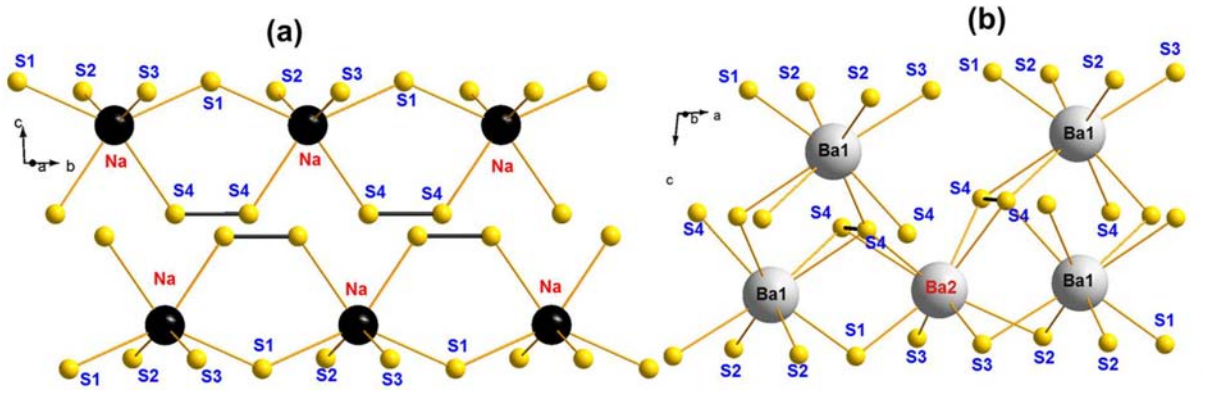

Figure 4. Coordination environment of (a) Na and (b) Ba(1), Ba(2) atoms including S−S bonds.

Band Structure Calculations. The electronic band structure of $NaBa_2Cu_3S_5$ in Figure 5 reveals an indirect band gap of 0.41

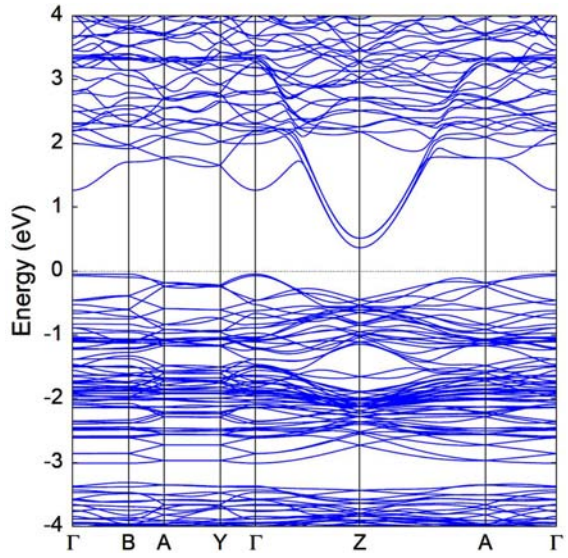

Figure 5. Calculated electronic band structure for $NaBa_2Cu_3S_5$.

eV between the Γ and Z points, which is in good agreement with the experimental band gap. The band structure shows highly anisotropic band dispersions, reflecting the two-dimensional layered structure of $NaBa_2Cu_3S_5$. For example, the valence bands show nearly flat dispersion along the Γ-B and A-Y directions which is perpendicular to the CuS_4 tetrahedral plane. On the other hand, the conduction and valence bands on the Y-Γ-Z plane are quite dispersive.

Charge Transport Properties. Electrical conductivity and Seebeck coefficient measurements were carried out on single crystals of $NaBa_2Cu_3S_5$. The electrical conductivity of this compound shows a typical behavior for a poor metal over the temperature range studied. As shown in Figure 6, the conductivity of $NaBa_2Cu_3S_5$ is ~450 S/cm at room temperature and increases to 1400 S/cm at 2 K. The room temperature Seebeck coefficient (Figure 7) of $NaBa_2Cu_3S_5$ is ~45 μV K^{-1}, indicating that the dominant charge carriers are holes (p-type).

Hall effect measurements were performed to estimate the concentration and mobility of carriers. Supporting Information, Figure S3 shows the magnetic field dependence of Hall resistivity ρ_H at different temperatures. In the experiment ρ_H was taken as $\rho_H = [\rho_{(+H)} - \rho_{(-H)}]/2$ for each point to eliminate

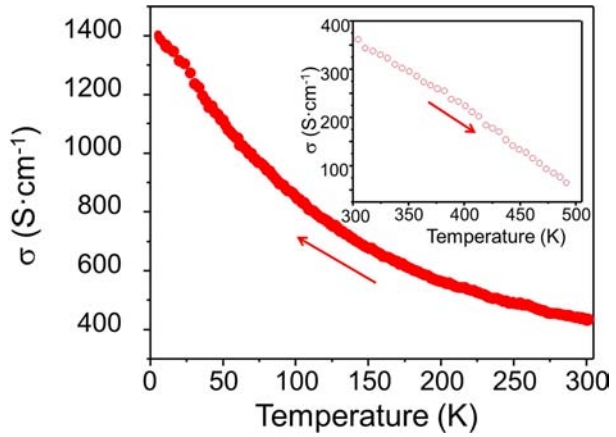

Figure 6. Electrical conductivity data as a function of temperature for single crystals of $NaBa_2Cu_3S_5$: low temperature region measured on a PPMS and high temperature region(inset figure) showing metallic behavior.

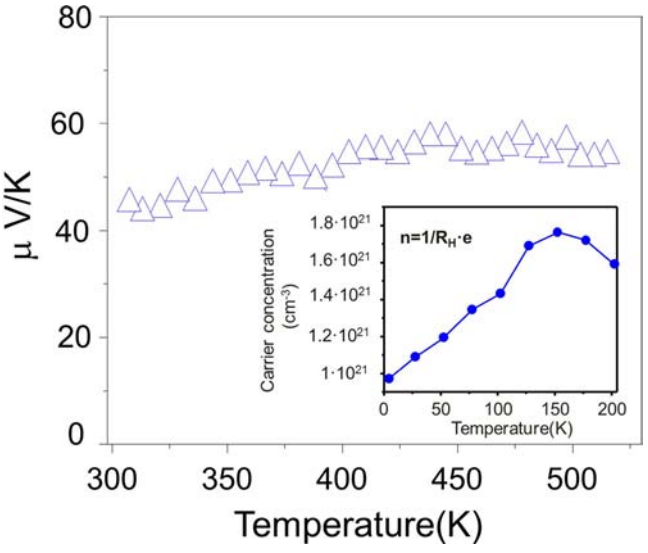

Figure 7. Variable-temperature thermoelectric power data for a single crystal sample of $NaBa_2Cu_3S_5$ showing a ***p*** type behavior. The inset figure shows carrier concentration as a function of temperature for $NaBa_2Cu_3S_5$.

any effect from misaligned of Hall electrodes. All curves in Supporting Information, Figure S3 have good linearity versus the magnetic field. Moreover, ρ_H is positive at all temperatures

dx.doi.org/10.1021/ic4008284 | Inorg. Chem. 2013, 52, 7210−7217

below 150 K giving a positive Hall coefficient $R_H = \rho_H/H$, which actually indicates that holes are the dominant charge carriers in the conduction of $NaBa_2Cu_3S_5$. The high carrier concentration (Figure 7, inset) found by Hall measurements of $p \sim 1.6 \times 10^{21}$ cm^{-3} at 200 K is indicative of *p*-type conduction and is consistent with the positive Seebeck coefficient. This number, however, may not be reliable given the single-band approximation that is typically made to estimate it. The hole mobility calculated from the Hall data and the electrical conductivity are moderate at about ~2 cm^2/V·s at 200 K.

The temperature-dependent magnetic susceptibility of $NaBa_2Cu_3S_5$, taken at H = 0.1 T over the range 5−300 K is shown in Supporting Information, Figure S4. The susceptibility is reminiscent of temperature-independent Pauli paramagnetism. At low temperatures, a paramagnetic increase of susceptibility is superposed with a diamagnetic component. This behavior was also reported for metallic $Ba_{1-x}K_xCu_2S_2$ synthesized from molten mixed Ba−K polysulfide salts[52] and KCu_4S_3.[72]

Since $NaBa_2Cu_3S_5$ is a valence-precise compound with an optical band gap of 0.45 eV (Figure 2b) it is interesting to ponder the origin of the observed metallic behavior in the charge transport properties. The metallic character is likely due to Cu vacancies. Assuming that one Cu atom vacancy creates one hole, for a hole concentration of 10^{21} cm^{-3} an amount of 4.41×10^{19} /cm^3 Cu vacancies, will be needed to account for them, this is approximately 0.13% Cu vacancies per unit cell. This small fraction in occupancy is too low to be reliably determined by single crystal refinement.

CONCLUDING REMARKS

The layered compound $NaBa_2Cu_3S_5$ is a narrow gap semiconductor with anti PbO-type $[Cu_2S_2]$ layers sandwiching a discrete disulfide unit. Despite its incongruent melting behavior we succeeded in growing millimeter size single crystals by slow cooling from the melt. The physical properties measured on single crystals show *p*-type metallic behavior, with moderately high electrical conductivity and carrier mobilities. In fact $NaBa_2Cu_3S_5$ is a degenerate semiconductor with high carrier concentration. Many copper chalcogenides are degenerate *p*-type semiconductors with relatively large numbers of holes in their valence band. Examples are BiCuOSe,[73] $La_{1-x}Sr_xCuOS$,[74] $LaCuOS_{1-x}Se_x$ with Mg doping[75] and BaCuTeF[76] chalcogenide-fluoride. These are wide gap materials and can exhibit good p-type conductivity and mobility.[77,78] Based on these phases further doping may be possible in $NaBa_2Cu_3S_5$ as well.

ASSOCIATED CONTENT

Supporting Information

Crystallographic data in CIF format. Further details are given in Figures S1−S4. This material is available free of charge via the Internet at http://pubs.acs.org.

AUTHOR INFORMATION

Corresponding Author

*E-mail: m-kanatzidis@northwestern.edu.

Notes

The authors declare no competing financial interest.

ACKNOWLEDGMENTS

This work is supported by the U.S. Department of Energy, Office of Basic Energy Sciences under contract no. DE-AC02-06CH11357.

REFERENCES

(1) Gabor, A. M.; Tuttle, J. R.; Albin, D. S.; Contreras, M. A.; Noufi, R.; Hermann, A. M. *Appl. Phys. Lett.* **1994**, *65*, 198.
(2) Kanatzidis, M. G.; Park, Y. *J. Am. Chem. Soc.* **1989**, *111*, 3767.
(3) (a) McCarthy, T. J.; Zhang, X.; Kanatzidis, M. G. *Inorg. Chem.* **1993**, *32*, 2944. (b) Liao, J. H.; Kanatzidis, M. G. *Chem. Mater.* **1993**, *5*, 1561.
(4) Peplinski, Z.; Brown, D.; Watt, T.; Hatfield, W.; Day, P. *Inorg. Chem.* **1982**, *21*, 1752.
(5) Burschka, C. *Z. Naturforsch. B* **1979**, *34*, 396.
(6) Brown, D. B.; Zubieta, J. A.; Vella, P. A.; Wrobleski, J. T.; Watt, T.; Hatfield, W. E.; Day, P. *Inorg. Chem.* **1980**, *19*, 1945.
(7) (a) Zhang, X.; Kanatzidis, M. G.; Hogan, T.; Kannewurf, C. R. *J. Am. Chem. Soc.* **1996**, *118*, 693. (b) Huang, S. P.; Kanatzidis, M. G. *Inorg. Chem.* **1991**, *30*, 1455.
(8) Boller, H. *J. Alloys Compd.* **2007**, *442*, 3.
(9) Klepp, K. O.; Sing, M.; Boller, H. *J. Alloys Compd.* **1992**, *184*, 265.
(10) Savelsberg, G.; Schaefer, H. *Z. Naturforsch.* **1978**, *33*, 711.
(11) Burschka, C. *Z. Anorg. Allg. Chem.* **1980**, *463*, 65−71.
(12) Klepp, K. O.; Sing, M.; Boller, H. *J. Alloys Compd.* **1993**, *198*, 25.
(13) Savelsberg, G.; Schaefer, H. *Mater. Res. Bull.* **1981**, *16*, 1291.
(14) Iglesias, J. E.; Pachali, K. E.; Steinfink, H. *Mater. Res. Bull.* **1972**, *7*, 1247.
(15) Burschka, C. B., W. *Z. Naturforsch.* **1977**, 32B.
(16) Klepp, K. O.; Sing, M. *Z. Kristallogr.: New Cryst. Struct.* **2002**, *217*, 474.
(17) Burschka, C. *Z. Anorg. Allg. Chem.* **1980**, *463*, 65.
(18) Klepp, K.; Yvon, K. *Acta Crystallogr.* **1980**, *B36*, 2389.
(19) Burschka, C.; Bronger, W. *Z. Naturforsch.* **1979**, *34B*, 675.
(20) Ohtani, T.; Hoshino, T.; Tsujinouchi, A.; Hasegawa, M.; Nagaoka, N.; Yokota, Y.; Okada, Y. *Mater. Res. Bull.* **1995**, *30*, 161.
(21) Gattow, G. *Acta Crystallogr.* **1957**, *10*, 549.
(22) Ohtani, T.; Ogura, J.; Sakai, M.; Sano, Y. *Solid State Commun.* **1991**, *78*, 504.
(23) Huster, J.; Bronger, W. *Z. Anorg. Allg. Chem.* **2001**, *627*, 1395.
(24) Berger, R. A. *J. Less-Common Met.* **1989**, *147*, 141.
(25) Iglesias, J. E.; Pachali, K. E.; Steinfink, H. *J. Solid State Chem.* **1974**, *9*, 6.
(26) Klepp, K.; Boller, H.; Voellenkle, H. *Monatsh. Chem.* **1980**, *111*, 727.
(27) Berger, R. A.; Eriksson, L. *J. Less-Common Met.* **1990**, *161*, 165.
(28) Effenberger, H.; Pertlik, F. *Monatsh. Chem.* **1985**, *116*, 921.
(29) Chang, J. S.; Hong, H. Y.-P.; Lee, G. H.; Wang, Y. *Mater. Res. Bull.* **1990**, *25*, 863.
(30) Zhang, X.; Park, Y.; Hogan, T.; Schindler, J. L.; Kannewurf, C. R.; Seong, S.; Albright, T.; Kanatzidis, M. G. *J. Am. Chem. Soc.* **1995**, *117*, 10300.
(31) Park, Y.; Kanatzidis, M. G. *Chem. Mater.* **1991**, *3*, 781.
(32) Munson, R. A.; DeSorbo, W.; Kouvel, J. S. *J. Chem. Phys.* **1967**, *47*, 1769.
(33) Meissner, W. *Z. Phys.* **1929**, *58*, 570.
(34) Shoenberg, D. *Nature* **1938**, *142*, 874.
(35) Fleming, R. M.; Ter Haar, L. W.; DiSalvo, F. *J. Phys. Rev. B* **1987**, *35*, 5388.
(36) Schilling, A.; Cantoni, M.; Guo, J. D.; Ott, H. R. *Nature* **1993**, *363*, 56.
(37) Cava, R. J.; Batlogg, B.; Krajewski, J. J.; Rupp, L. W.; Schneemeyer, L. F.; Siegrist, T.; Vandover, R. B.; Marsh, P.; Peck, W. F.; Gallagher, P. K.; Glarum, S. H.; Marshall, J. H.; Farrow, R. C.; Waszczak, J. V.; Hull, R.; Trevor, P. *Nature* **1988**, *336*, 211.
(38) Bednorz, J. G.; Müller, K. A. *Z. Phys. B: Condens. Matter* **1986**, *64*, 189.
(39) Orenstein, J.; Millis, A. J. *Science* **2000**, *288*, 468.

(40) Kamihara, Y.; Watanabe, T.; Hirano, M.; Hosono, H. *J. Am. Chem. Soc.* **2008**, *130*, 3296.
(41) Christianson, A. D.; Goremychkin, E. A.; Osborn, R.; Rosenkranz, S.; Lumsden, M. D.; Malliakas, C. D.; Todorov, I. S.; Claus, H.; Chung, D. Y.; Kanatzidis, M. G.; Bewley, R. I.; Guidi, T. *Nature* **2008**, *456*, 930.
(42) Avci, S.; Chmaissem, O.; Goremychkin, E. A.; Rosenkranz, S.; Castellan, J. P.; Chung, D. Y.; Todorov, I. S.; Schlueter, J. A.; Claus, H.; Kanatzidis, M. G.; Daoud-Aladine, A.; Khalyavin, D.; Osborn, R. *Phys. Rev. B* **2011**, *83*, 172503.
(43) Avci, S.; Chmaissem, O.; Chung, D. Y.; Rosenkranz, S.; Goremychkin, E. A.; Castellan, J. P.; Todorov, I. S.; Schlueter, J. A.; Claus, H.; Daoud-Aladine, A.; Khalyavin, D. D.; Kanatzidis, M. G.; Osborn, R. *Phys. Rev. B* **2012**, *85*, 184507.
(44) Bud'ko, S. L.; Sturza, M.; Chung, D. Y.; Kanatzidis, M. G.; Canfield, P. C. *Phys. Rev. B* **2013**, *87*, 100509.
(45) Li, W.; Ding, H.; Deng, P.; Chang, K.; Song, C. L.; He, K.; Wang, L. L.; Ma, X. C.; Hu, J. P.; Chen, X.; Xue, Q. K. *Nat. Phys.* **2012**, *8*, 126.
(46) Zhang, A. M.; Xia, T.-l.; Liu, K.; Tong, W.; Yang, Z.-r.; Zhang, Q.-m. *Sci. Rep.* **2013**, *3*, 1216.
(47) Tianping, Y.; Xiaolong, C.; Gang, W.; Shifeng, J.; Xiaofang, L.; Tingting, Z.; Han, Z.; Shijie, S.; Wanyan, W. *J. Am. Chem. Soc.* **2013**, *135*, 2951.
(48) Shoemaker, D. P.; Chung, D. Y.; Claus, H.; Francisco, M. C.; Avci, S.; Llobet, A.; Kanatzidis, M. G. *Phys. Rev. B* **2012**, *86*, 184511.
(49) Buckel, W.; Hilsc, R. *Z. Phys.* **1950**, *128*, 324.
(50) Bither, T. A.; Prewitt, C. T.; Gillson, J. L.; Bierstedt, P. E.; Flippen, R. B.; Young, H. S. *Solid State Commun.* **1966**, *4*, 533.
(51) Hagino, T.; Seki, Y.; Wada, N.; Tsuji, S.; Shirane, T.; Kumagai, K.; Nagata, S. *Phys. Rev. B* **1995**, *51*, 12673.
(52) Zhang, X.; Hogan, T.; Kannewurf, C. R.; Kanatzidis, M. G. *J. Alloys Compd.* **1996**, *236*, 1.
(53) Mouallem-Bahout, M.; Potel, M.; Halet, J. F.; Padiou, J.; Carel, C.; Retat-Saveleva, M. *Eur. J. Solid State Inorg. Chem.* **1996**, *33*, 483.
(54) *X-AREA; X-SHAPE; X-RED*; STOE & Cie GmbH:: Darmstadt, Germany, 2004.
(55) Sheldrick, G. M. *SHELXTL*, version 5.1; University of Göttingen: Göttingen, Germany, 1997.
(56) Petricek, V.; Dusek, M.; Palatinus, L. *Jana2006, The crystallographic computing system*; Institute of Physics: Praha, Czech Republic, 2006.
(57) Carvajal, R. *J. Phys. Rev. B* **1993**, *55*, 192.
(58) Kortum, G.; Braun, W.; Herzog, G. *Angew. Chem.* **1963**, *75*, 653.
(59) Larson, P.; Mahanti, S. D.; Kanatzidis, M. G. *Phys. Rev. B* **2000**, *61*, 8162.
(60) McCarthy, T. J.; Tanzer, T. A.; Kanatzidis, M. G. *J. Am. Chem. Soc.* **1995**, *117*, 1294.
(61) Trikalitis, P. N.; Rangan, K. K.; Bakas, T.; Kanatzidis, M. G. *J. Am. Chem. Soc.* **2002**, *124*, 12255.
(62) Wood, C.; Chmielewski, A.; Zoltan, D. *Rev. Sci. Instrum.* **1988**, *59*, 951.
(63) Blöchl, P. E. *Phys. Rev. B* **1994**, *50*, 17953.
(64) Kresse, G.; Hafner, J. *J. Phys. B: Condens. Matter* **1994**, *6*, 8245.
(65) Kresse, G.; Furthmüller, J. *Phys. Rev. B* **1996**, *54*, 11169.
(66) Takeuchi, K.; Kudoh, Y.; Sato, G. *Z. Kristallogr.* **1985**, *173*, 119.
(67) Fjellvag, H.; Gronvold, F.; Stolen, S.; et al. *Z. Kristallogr.* **1988**, *184*, 111.
(68) Janz, G. J.; Coutts, J. W.; Downey, J. R.; Roduner, E. *Inorg. Chem.* **1976**, *15*, 1755.
(69) Shoemaker, D. P.; Chung, D. Y.; Mitchell, J. F.; Bray, T. H.; Soderholm, L.; Chupas, P. J.; Kanatzidis, M. G. *J. Am. Chem. Soc.* **2012**, *134*, 9456.
(70) Janz, G. J.; Downey, J. R.; Roduner, E.; Wasilczyk, G. J.; Coutts, J. W.; Eluard, A. *Inorg. Chem.* **1976**, *15*, 1759.
(71) El Jaroudi, O.; Picquenard, E.; Demortier, A.; Lelieur, J.; Corset, J. *Inorg. Chem.* **1999**, *38*, 2394.
(72) Schramm, C. J.; Scaringe, R. P.; Stojakovic, D. R.; Hoffman, B. M.; Ibers, J. A.; Marks, T. J. *J. Am. Chem. Soc.* **1980**, *102*, 6702.
(73) Tate, J.; Newhouse, P. F.; Kykyneshi, R.; Hersh, P. A.; Kinney, J.; McIntyre, D. H.; Keszler, D. A. *Thin Solid Films* **2008**, *516*, 5795.
(74) Ueda, K.; Inoue, S.; Hirose, S.; Kawazoe, H.; Hosono, H. *Appl. Phys. Lett.* **2000**, *77*, 2701.
(75) Hiramatsu, H.; Ueda, K.; Ohta, H.; Hirano, M.; Kamiya, T.; Hosono, H. *Thin Solid Films* **2003**, *445*, 304.
(76) Park, C. H.; Kykyneshi, R.; Yokochi, A.; Tate, J.; Keszler, D. A. *J. Solid State Chem.* **2007**, *180*, 1672.
(77) Yanagi, H.; Tate, J.; Park, S.; Park, C. H.; Keszler, D. A.; Hirano, M.; Hosono, H. *J. Appl. Phys.* **2006**, *100*, 83705.
(78) Inoue, S.; Ueda, K.; Hosono, H.; Hamada, N. *Phys. Rev. B* **2001**, *64*, 245211.